Aerodynamics Improvement of NACA 0015 by Using Co-Flow Jet

James Julian[1], Waridho Iskandar[2], Fitri Wahyuni[3]
(Received: 21 November 2022 / Revised: 11 December 2022 / Accepted: 17 December 2022)

***Abstract*— this study analyzes co-flow as active flow control in the object of the airfoil. NACA 0015 is the airfoil used in this study. The airfoil was then modified to add co-flow jet features. Co-flow jet was placed on the upper chamber to analyze its effect on airfoil performance. Further, the Co-flow jet was studied by varying the injected mass flow rate ($\dot{m}$) in the injection slot. The variation of $\dot{m}$ is 0.15, 0.20, and 0.25 kg/s. The study used CFD with the governing equation RANS. Reynolds Averaged Navier Stokes combined with turbulence model to solve all equations. Two equations for the turbulence model are used in this study. Specifically, this study discusses the aerodynamics of the airfoil, i.e., lift force, drag force, and fluid flow visualization, such as pressure contour and velocity contour. Co-flow jets can improve the aerodynamics of airfoils. The bigger the $\dot{m}$ injected, the higher the lift coefficient increases. On the other hand, the drag force will be reduced as the number of injected fluid flow increases. Because of that, the airfoil efficiency will be better if using a co-flow jet. However, the C_l/C_d curve peak shifts to smaller as the injection fluid flow are bigger. The fluid flow visualization by velocity contour on AoA=20° revealed that the co-flow jet could overcome separation.**

Keywords—co-flow jet, mass flow rate, aerodynamic performance, NACA 0015.

I. INTRODUCTION

The aerodynamic capability of the airfoil is one of the crucial factors in determining its quality of the airfoil. When applied to various equipment that supports human life, aerodynamics itself plays an important role [1]. The efficiency and flight capability of the aircraft depend on the aerodynamic capabilities of the airfoil or wing used. If the airfoil used is not reliable, it will be very detrimental. For example, if an aircraft has a large C_d, the aircraft will experience a large drag force so that fuel use efficiency is reduced. On the other hand, if the aircraft does not have a good enough lift and stalls quickly, the aircraft becomes unreliable and has very limited flying capabilities. One of the most significant limitations of the airfoil is the separation [2].

Fluid flow separation can make C_d airfoil increase [3][4]. Further, the separation can also cause the airfoil to undergo a very drastic decrease in C_l which is called stall [5]. To overcome the problem of fluid flow separation, ideas about fluid flow control devices emerged [6][7]. Plasma actuators, synthetic jets, vortex generators, and co-flow jets are examples of fluid flow control devices [8][9].

The fluid flow control device can reduce the separation with different capabilities. The Co-flow Jet is a flow control device that can significantly positively impact the airfoil. Co-flow jets can be classified as active flow control devices [11] [12].

Several studies have revealed and described co-flow jets as flow control devices. One of these studies discusses co-flow jets for fluid flow with a Reynolds number of 200,000. Co-flow jets are applied to the Clark Y-M18 airfoil. The study was carried out computationally and experimentally. The results of computational and experimental studies show that co-flow jets can improve the aerodynamics of airfoils. The use of a co-flow jet can increase C_l and delay stall. Moreover, the co-flow jet can minimize C_d so that the airfoil can work more efficiently [13].

Another study showed similar results where co-flow jets can produce C_l better than baseline airfoils. Co-flow jets can also increase C_{lmax}. The increase in C_{lmax} varies depending on the location of the fluid injection. If injection slot is placed in 6%-13% chord (c) and the suction slot is placed in 82% c, the C_{lmax} can increase about 3.6% to 31.9%. If the suction location is shifted to 85% of the chord length, the increase in C_{lmax} can be obtained at 2.58%-29.32%. The co-flow jets can also overcome fluid flow separation, as in the study conducted by Gias et al., (2014). It is illustrated by the fluid flow streamline that at NACA 0015, the fluid flow recirculation can be removed at AoA=19º. This is very different from the airfoil condition without a co-flow jet, where the separation has been wholly formed even at a smaller AoA of 14° [15].

From the various studies above, it can be concluded that co-flow jets can provide satisfactory results in fluid flow control and overcome fluid flow separation problems. However, the above discussion has not specifically discussed the $\dot{m}$ of the injected fluid. Therefore, this study will identify precisely the effect of the injected $\dot{m}$ on improving the aerodynamic performance of NACA 0015. This study also reveals that it can be used as complementary data and references for other flow control studies.

James Julian is with Department of Mechanical Engineering, Universitas Pembangunan Nasional Veteran Jakarta, Jakarta, 12450, Indonesia. E-mail: zames@upnvj.ac.id
Waridho Iskandar is with Department of Mechanical Engineering, Universitas Pembangunan Nasional Veteran Jakarta, Jakarta, 12450, Indonesia. E-mail: waridho.iskandar@upnvj.ac.id
Fitri Wahyuni is with Department of Mechanical Engineering, Universitas Pembangunan Nasional Veteran Jakarta, Jakarta, 12450, Indonesia. E-mail: fitriwahyuni@upnvj.ac.id

II. METHOD

A. Co-flow Jet

Co-flow jet is a device that usually placed on the airfoil's upper chamber. This flow control device consists of a suction slot and injection slot. In the near of leading edge of the airfoil, there is an injection slot. In the near of the trailing edge, there is a suction slo [16] t. Co-flow jet is an active flow control device that can be classified as ZNMF or zero-net mass flux therefore the injected and inhaled fluid flow must be same [17]. Co-flow jet works by sucking and injecting fluid. Thus, there is a mass of injected fluid. The injected fluid mass can then fill the vacuum in the event of separation of the fluid flow [18]. In this study, three variations of $\dot{m}$ were proposed, namely 0.15, 0.20 and 0.25 kg/s. An overview of the Co-flow jet is in Figure 1.

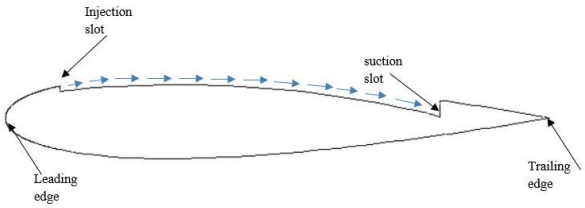

Figure. 1. Co-flow jet on airfoil

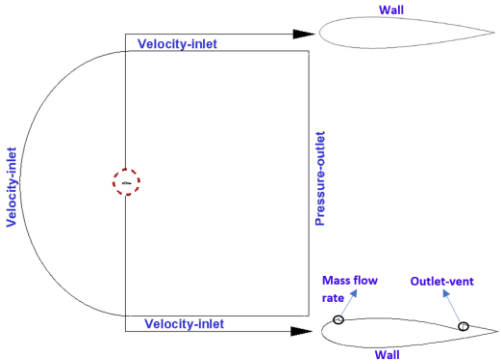

Figure. 2. Boundary condition

B. Pre-processing

Pre-processing is the preparatory stage before the computational process is carried out. Pre-processing consists of the stages of making geometry, boundary conditions, and meshing [19]. In this study, two geometries were made, i.e., baseline NACA 0015 and NACA 0015, which had been given injection slots and suction slots. *c* value of the airfoil is 1 m. In this study, the domain consists of two different parts. The first part is velocity-inlet and the second part is pressure-outlet. The entire surface of the baseline airfoil is made as a wall (no slip). Meanwhile, for airfoils with co-flow jets, the boundary condition for the injection slot is the $\dot{m}$. On the other hand, the boundary condition in the suction slot is the vent outlet. The dimensions of the domain and its boundary conditions can be seen in Figure 2. Each airfoil in a domain with the shape and size is shown in Figure 3.

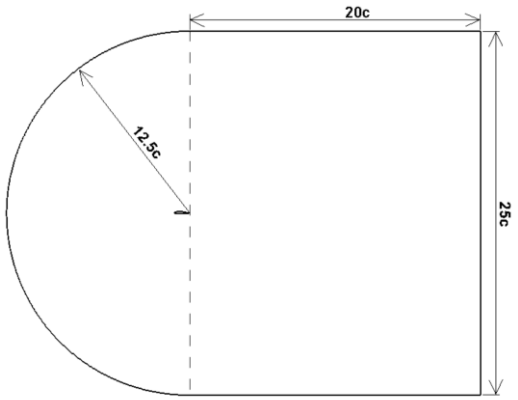

(a) Domain

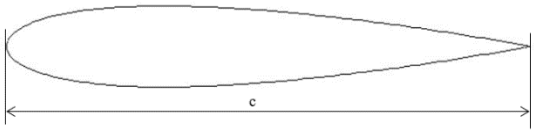

(b) Baseline NACA 0015

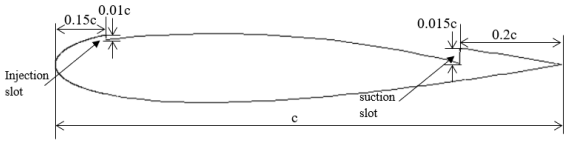

(c) NACA 0015 with co-flow jet

Figure. 3. Detail geometries.

After setting all of the geometry, meshing is the next step of the computational process. Meshing can be defined as the computation step where the domain geometry is divided into smaller parts to calculate. Each part of the mesh is known as a mesh element. In two-dimensional computation, there are only two types of mesh elements. The first type of element is quadrilateral. This element is very suitable if used in structured mesh because it offers a lower cost per iteration than another element mesh. Another element of mesh is triangle mesh, which is very easy to implement even on complex geometry, so this mesh element is usually used in the unstructured mesh. Mesh variations proposed in this study are 5×10^4, 10^5 dan 2×10^5. The mesh independence test tested these variations to determine the most efficient mesh. The most efficient mesh is then used to calculate further computation process. The type of mesh used in this study is structured mesh. Meanwhile, each element of mesh is set to form a quadrilateral element. The mesh is made closer to the surface of the airfoil to capture various fluid flow phenomena in the near of airfoil [20]. More specific information are given on Figure 4.

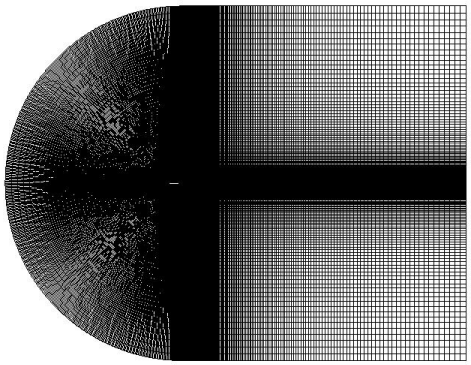

(a) Domain

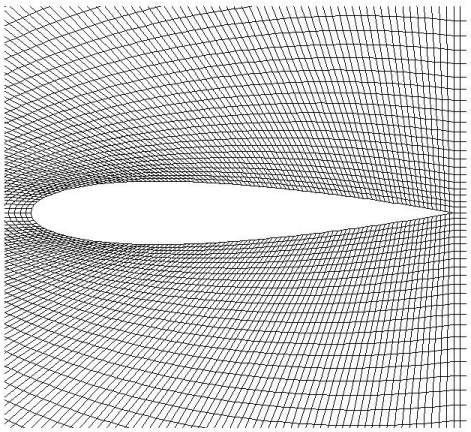

(b) around baseline NACA 0015

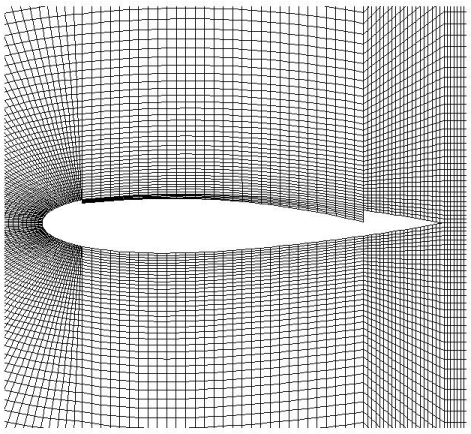

(c) NACA 0015 with co-flow jet
Figure. 4. Mesh in this study.

C. Solving method

The governing equation to solve the fluid flow problem in this study is the RANS. The fluid flow condition is modeled as a steady fluid. This study used $k-\omega$ as turbulence model. It chosen because very suitable for low and medium Reynolds number. The mathematical equations for the regulating equation are written in equations 1 and 2 [21]. The equations are solved by the Pressure based coupled algorithm. Changes in the AoA of the airfoil are correspond to vectors x and y [22]. In this study, NACA 0015 is simulated on the Reynolds number 360000.

$$\frac{\partial \rho}{\partial t}+\frac{\partial}{\partial x_i}(\rho u_i)=0 \tag{1}$$

$$\frac{\partial}{\partial t}(\rho u_i)+\frac{\partial}{\partial x_i}(\rho u_i u_j)=\frac{\partial p}{\partial x_i}+\frac{\partial}{\partial x_j}\left[\mu\left(\frac{\partial u_i}{\partial x_j}+\frac{\partial u_j}{\partial x_i}-\frac{2}{3}\delta_{ij}\frac{\partial u_i}{\partial x_i}\right)\right]+\frac{\partial}{\partial x_i}\left(-\rho\overline{u_i' u_j'}\right) \tag{2}$$

D. Post-processing

Post-processing is the final stage of the computational process. The post-processing stage is done by displaying data from CFD. The resulting data can be in the form of fluid aerodynamics data. In addition to aerodynamic data, the post-processing stage is also carried out with fluid flow visualization data. Fluid flow visualization can be displayed on contour and streamlines [23].

E. Aerodynamic of airfoil

The first discussion is about aerodynamic forces. The aerodynamics of the airfoil is the main point of view to assess the ability of the co-flow jet as active flow control. Two aerodynamic forces are commonly discussed, i.e., drag and lift forces [24]. The drag force can be defined as the aerodynamic forces in which the direction of the force is parallel to the fluid flow vector [25]. Meanwhile, the lift force can be said as the aerodynamic force that the vector is perpendicular to the fluid flow direction. Drag and lift forces are commonly written as dimensionless values, known as coefficient drag and coefficient lift. Both of them mentioned in equations 3 and 4, respectively [26].

$$C_d=\frac{2d}{\rho u^2 c} \tag{3}$$

$$C_l=\frac{2l}{\rho u^2 c} \tag{4}$$

Whereas
C_d : coefficient of drag

C_l : coefficient of lift
c : chord length
d : drag force
l : lift force
u : free-stream velocity
ρ : density of fluid

III. Results and Discussion

Mesh variations in this study must be checked to ensure that all mesh is in range convergence. Further, the error value of each mesh also has to be determined. There is one method of mesh independence test that can do it simultaneously [27]. The method is called Richardson Extrapolation. Richardson Extrapolation is generalized by Roache. Each stage of the mesh independence test was carried out in the same way as in the study by Iskandar et al [28]. The mesh independence test results will be discussed more comprehensively in this paragraph. The mesh independence test was conducted using velocity around the airfoil in positions x=0.5 and y=0.15. The ratio of mesh variations in this study is 2. Meanwhile, in this mesh independence test, the order is 1.8690. The calculation results in the grid convergence index for fine and coarse mesh with the values of 0.0540% and 0.1955%, respectively. The safety factor used for the mesh independence test is 1.25. The value of relative error is 0.0011. 1.0059 is the final results of mesh independence test, so it can be concluded the mesh variation in the convergence index. The parameter value is 5.896. Overall, the results are given in Figure 5. Fine mesh gives the closest value to the parameter; therefore, this mesh will be used for further computation.

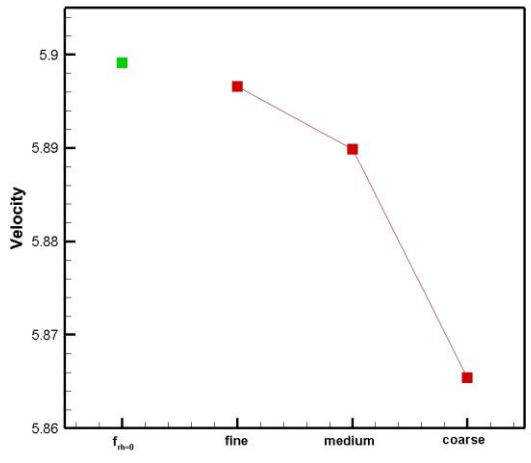

Figure. 5. Mesh independence test results

Figure 6 describes the change in the distribution of C_l to changes in AoA. Before discussing further airfoil data with co-flow jets, the first step is to compare CFD results to experiment results [29]. The CFD results are similar to experimental results. The computational data shows good results, especially in the small AoA values. The computational results show that the stall is predicted to be 1° faster than the computational results. After experiencing a stall, the larger the AoA, the more identical the data will be to each other. The use of a co-flow jet has been proven to increase C_l of NACA015. Besides increasing C_l, co-flow jets are also effective at delaying stalls. The higher the $\dot{m}$, the more significant the increase in C_l produced. The increase in C_l becomes very significant when at AoA≥10°. Increasing the injection $\dot{m}$ can also delay the stall even further. Stall at the injection $\dot{m}$ of 0.15kg/s occurred at AoA=18°. When the $\dot{m}$ is 0.20 kg/s, a stall occurs at AoA=20°. Meanwhile, when the $\dot{m}$ increases to 0.25 kg/s, the stall becomes more and more delayed until it finally occurs at AoA=22°.

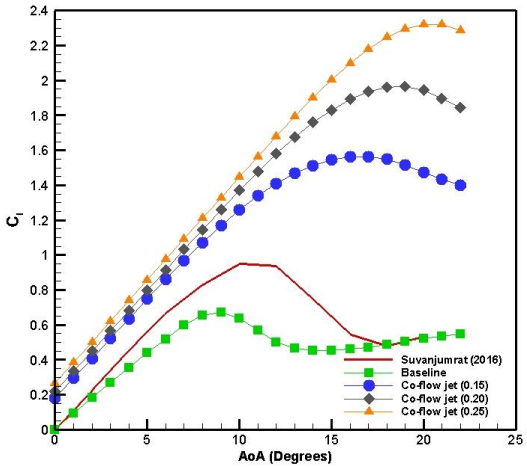

Figure. 6. C_l of the airfoil

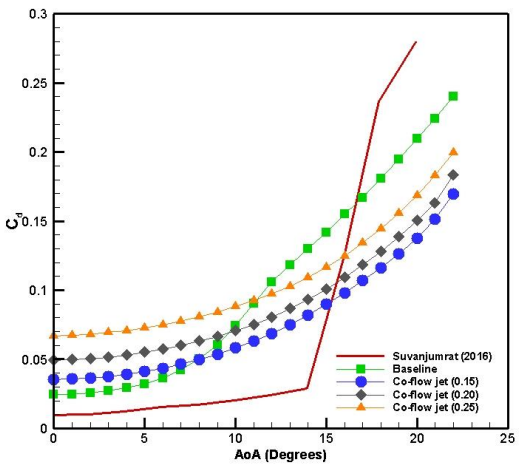

Figure. 7. C_d of the airfoil

The C_d curve for changes in AoA can be seen in Figure 7. Similar to C_l, experimental and computational C_d at baseline NACA 0015 showed results that were not much different for AoA, which was relatively small. A co-flow jet at AoA≤8° has a negative impact, namely increasing C_d in the NACA 0015 airfoil. However, if AoA>8°, then

the co-flow jet begins to show a positive effect; when AoA=9° C_d produced by the airfoil has been given a co-flow jet with the injection of 0.15 kg/s has been smaller than the baseline NACA 0015. For a co-flow jet with $\dot{m}$ of 0.2 kg/s, when the AoA≥10° C_d produced starts to be smaller than the baseline NACA 0015. If the $\dot{m}$ is 0.25 kg/s, the C_d of the co-flow jet becomes smaller than the baseline C_d of NACA 0015 when AoA>11°. Overall, the increase $\dot{m}$ in the co-flow jet increased C_d.

A C_l/C_d curve plot for the AoA changes is made in Figure 8. The C_l/C_d curve can be used as a reference to determine at what angle of attack the airfoil gets the best performance. Baseline NACA 0015 gets its best performance at AoA=6°, with the peak of the curve at 14.2. Meanwhile, on a co-flow jet with the injection of 0.15 kg/s, the best performance of the airfoil is when AoA=13°. When the $\dot{m}$ increases, the effective AoA shifts to a smaller AoA. When $\dot{m}$ is 0.20 kg/s, the airfoil gets its best performance at AoA=11°. If $\dot{m}$ is enlarged to 0.25 kg/s, the airfoil gets its best performance when AoA=9°.

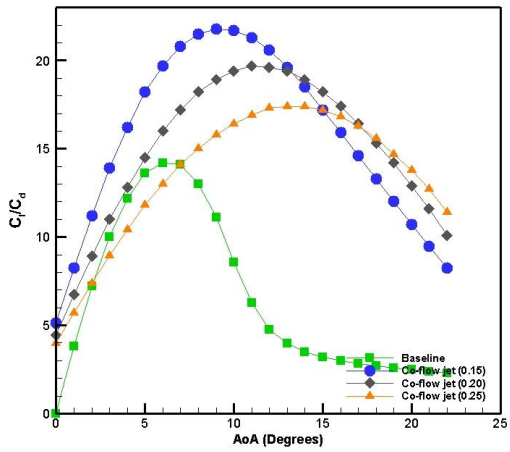

Figure. 8. C_l/C_d curve of the airfoil

Visualization of fluid flow, as shown in Figure 9, is made to see the effect of the co-flow jet in controlling fluid flow on the upper chamber. The figure shows that the velocity contour and fluid flow streamline are at AoA=20°. Figure 9 (a) is the contour and streamline of fluid flow at baseline NACA 0015. The separation is very clearly seen in Figure 9(a). Co-flow jets have proven to be very effective in solving fluid flow separation problems; this can be seen in Figures 9(b), 9(c), and 9(d). Overall, there is no significant difference between the three variations of $\dot{m}$ when viewed from the fluid flow streamline. The only visible difference is the streamline near the trailing edge. The streamline is slightly upward when the injection fluid flow is 0.15 kg/s. This can be corrected when the injection fluid flow increases to 0.20 kg/s. If we look at the velocity contour, it can be seen that the low-velocity area near the trailing edge is frequently decreasing with increasing injection fluid flow value. The fluid flow velocity contour below the leading shows the opposite result from the trailing edge. When the airfoil is without a co-flow jet, the low-velocity flow is relatively smaller when compared to the airfoil with a co-flow. This low-velocity area will expand as the $\dot{m}$ increases.

The following visualization is pressure around the airfoil. The airfoil has a particular characteristic where the fluid velocity on the upper chamber can be accelerated. According to the Bernoulli principle, if the fluid velocity increases, the pressure will be decreased. In other words, fluid flow's velocity and pressure are inverses. However, the velocity acceleration occurs on the lower chamber. Therefore, if the AoA of the airfoil is equal to zero, the airfoil loses its ability to generate lift. Meanwhile, if the AoA of the airfoil is greater than zero, the airfoil can generate lift force. Figure 10 is the pressure contour around the airfoil when the AoA is equal to 20º. Figure 10 also shows that the fluid pressure in upper chamber is lower than in the lower chamber. Hence, the lift force can generate in this AoA. The co-flow jet can decrease the pressure on the upper chamber. If the fluid injection on the upper chamber increases, meanwhile there is a decrease pressure in the upper chamber. Pressure distribution changes also occur on the lower chamber. The changes on the lower camber inversely from the upper chamber where the increases in the fluid injection cause the pressure on the lower chamber. It is why the greater the injection fluid, the bigger the C_l produced by the airfoil.

IV. Conclusion

This research reveals that co-flow jet has its ability to upgrade the capabilities of NACA 0015 with further increases depending on the $\dot{m}$ following through the injection slot. The higher the injection, the more significant the increase in C_l and the more delayed stall. Meanwhile, in terms of C_d, the co-flow jet can reduce C_d at AoA>8°. If the $\dot{m}$ increases, the C_d will also increase so that the drag force becomes large. Based on the plot of the C_l/C_d curve for changes in AoA, it can be concluded that increasing the injection fluid flow will reduce the effective AoA. When the $\dot{m}$ is 0.15, the effective AoA of the airfoil is 13°, but when the $\dot{m}$ is increased to 0.20 kg/s, the effective AoA is 11°, and if the $\dot{m}$ is increased again, the effective AoA is 9°. Overall, it can be concluded that the $\dot{m}$ of 0.15 is good enough to use compared to 0.2 kg/s or 0.25 kg/s. Based on velocity contours and flow streamlines, co-flow jets can solve the problem of recirculating flow on the upper chamber at AoA=20°. The recirculating flow on the upper chamber disappears when the co-flow jet is used.

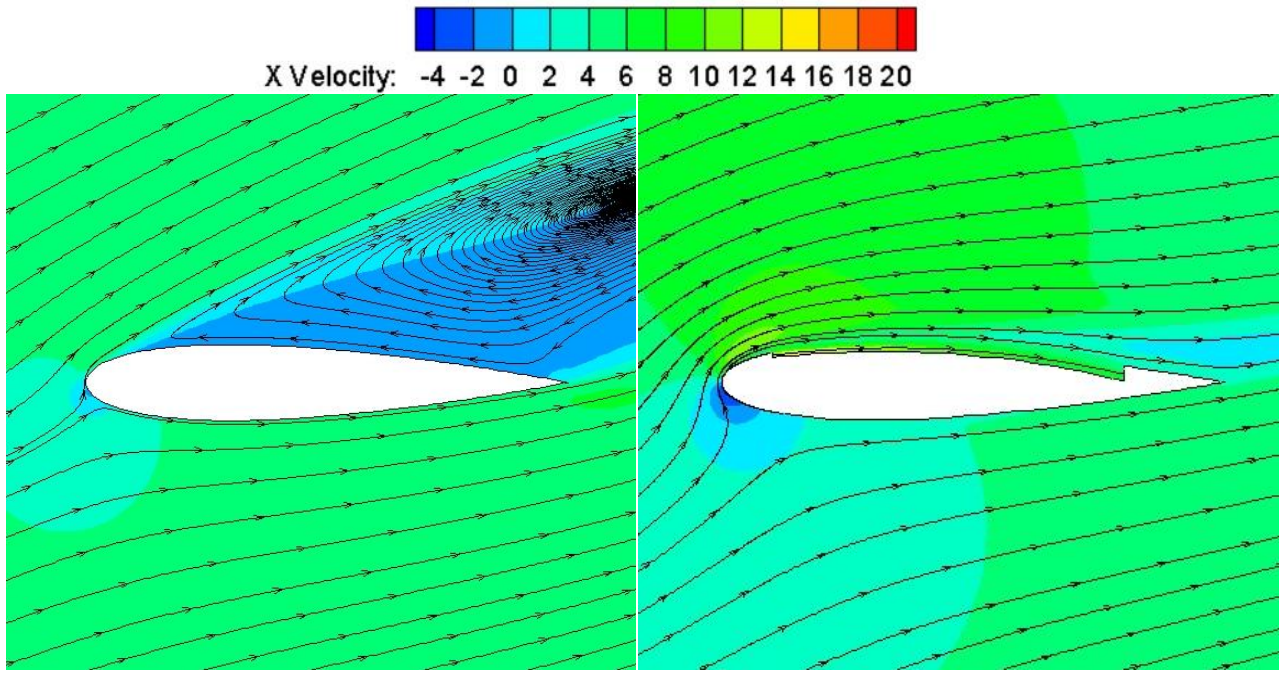

(a) Baseline NACA 0015 (b) Co-flow jet with injection 0.15 kg/s

(c) Co-flow jet with injection 0.20 kg/s (d) Co-flow jet with injection 0.25 kg/s

Fig. 9. Velocity contour and streamline

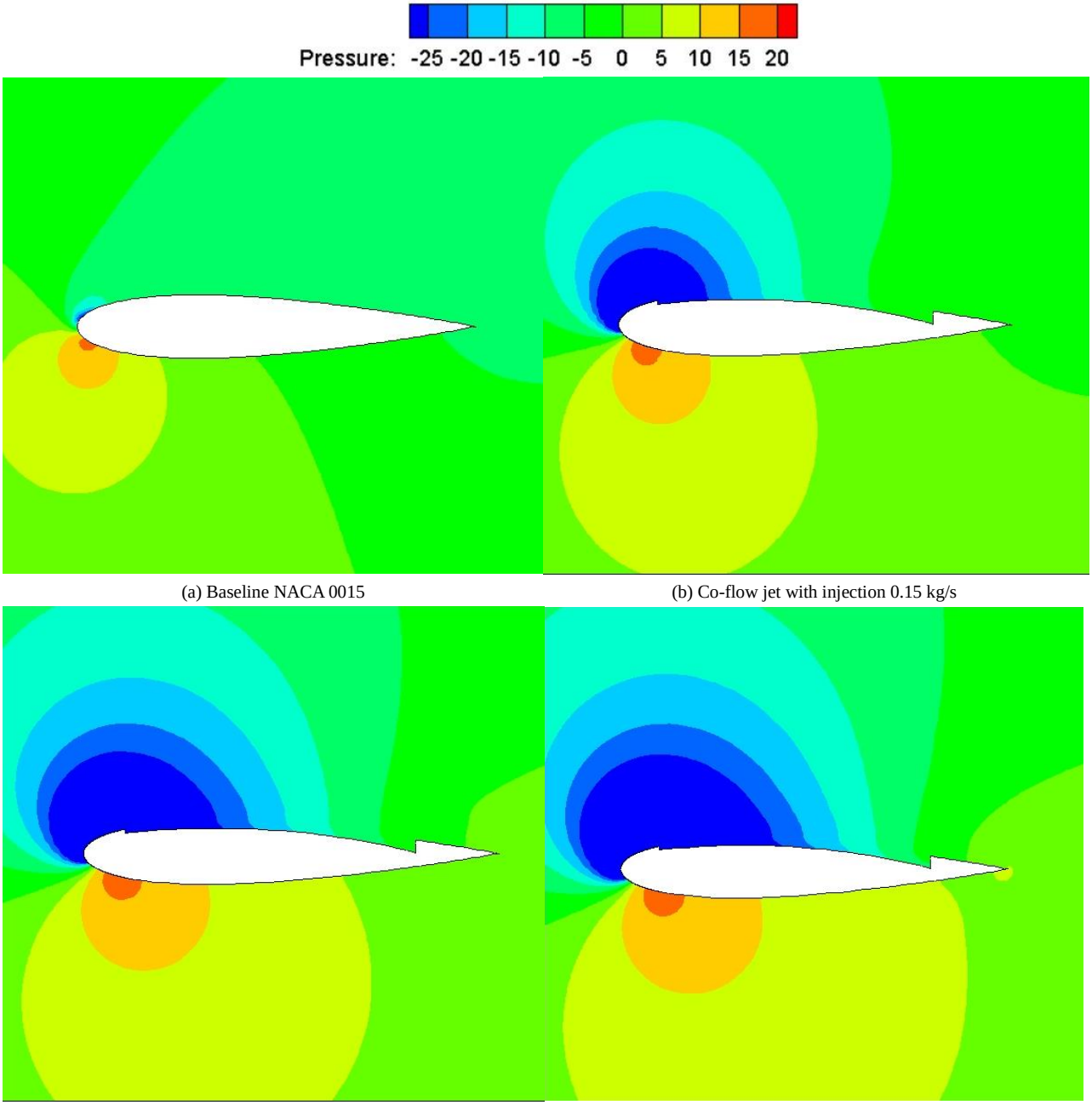

(a) Baseline NACA 0015

(b) Co-flow jet with injection 0.15 kg/s

(c) Co-flow jet with injection 0.20 kg/s

(d) Co-flow jet with injection 0.25 kg/s

Fig. 10. Pressure contour

REFERENCES

[1] J. Julian, Harinaldi, Budiarso, C.-C. Wang, and M.-J. Chern, "Effect of plasma actuator in boundary layer on flat plate model with turbulent promoter," *Proc Inst Mech Eng G J Aerosp Eng*, vol. 232, no. 16, pp. 3001–3010, 2018.

[2] F. C. Megawanto, R. F. Karim, N. T. Bunga, and J. Julian, "Flow separation delay on NACA 4415 airfoil using plasma actuator effect," *International Review of Aerospace Engineering*, vol. 12, no. 4, pp. 180–186, 2019.

[3] J. Julian, R. Difitro, and P. Stefan, "The effect of plasma actuator placement on drag coefficient reduction of Ahmed body as an aerodynamic model," *International Journal of Technology*, vol. 7, no. 2, pp. 306–313, 2016.

[4] Harinaldi, Budiarso, and J. Julian, "The effect of plasma actuator on the depreciation of the aerodynamic drag on box model," in *AIP Conference Proceedings*, 2016, vol. 1737, no. 1, p. 040004.

[5] J. Julian, H. Harinaldi, and B. Budiarso, "THE EFFECT OF PLASMA ACTUATOR UTILIZATION TO THE REDUCTION OF AERODYNAMIC DRAG OF CYLINDER AND BOX MODELS," 2016. Accessed: Dec. 09, 2022. [Online]. Available: http://hdl.handle.net/2263/61963

[6] F. C. Megawanto, Harinaldi, Budiarso, and J. Julian, "Numerical analysis of plasma actuator for drag reduction and lift enhancement on NACA 4415 airfoil," in *AIP Conference Proceedings*, 2018, vol. 2001, no. 1, p. 050001.

[7] R. F. Karim and J. Julian, "Drag reduction due to recirculating bubble control using plasma actuator on a squareback model," in *MATEC Web of Conferences*, 2018, vol. 154, p. 01108.

[8] V. Maldonado, N. Peralta, S. Gorumlu, and W. Ayele, "On the figure of merit and streamwise flow of a propulsive rotor with synthetic jets," *Aerosp Sci Technol*, vol. 113, p. 106712, 2021, doi: https://doi.org/10.1016/j.ast.2021.106712.

[9] E. A. Kosasih, R. F. Karim, and J. Julian, "Drag reduction by combination of flow control using inlet disturbance body and plasma actuator on cylinder model," *Journal of Mechanical Engineering and Sciences*, vol. 13, no. 1, pp. 4503–4511, 2019.

[10] J. Julian and R. F. Karim, "Flow control on a squareback model," *International Review of Aerospace Engineering*, vol. 10, no. 4, pp. 230–239, 2017.

[11] Y. Yang and G. Zha, "Super-Lift Coefficient of Active Flow Control Airfoil: What is the Limit?," in *55th AIAA Aerospace Sciences Meeting*, American Institute of Aeronautics and Astronautics, 2017. doi: doi:10.2514/6.2017-1693.

[12] W. Harinaldi, S. Adhika, and J. Julian, "The comparison of an analytical, experimental, and simulation approach for the average induced velocity of a dielectric barrier discharge (DBD)," in *The 10th International Meeting of Advances in Thermofluids (IMAT 2018): Smart City: Advances in Thermofluid Technology in Tropical Urban Development*, 2019, vol. 2062, no. 1, p. 020027.

[13] S. Zhang, X. Yang, B. Song, and J. Xu, "Numerical and Experimental Study of the Co-Flow Jet Airfoil Performance Enhancement," in *55th AIAA Aerospace Sciences Meeting*, American Institute of Aeronautics and Astronautics, 2017. doi: doi:10.2514/6.2017-1694.

[14] C. M. Vigneswaran and V. Kumar GC, "AERODYNAMIC PERFORMANCE ANALYSIS OF CO-FLOW JET AIRFOIL," *International Journal of Aviation, Aeronautics, and Aerospace*, vol. 8, no. 1, p. 10, 2021.

[15] M. Robiul awal Tanvir, M. Tanvir Ibny Gias, M. Mahmudul Hasan, M. Amzad Hossain, and M. Mashud, "Flow Separation Control on a NACA 2415 Airfoil using Co-Flow Jet (CFJ) Flow Flow Separation Control on a NACA 0015 Airfoil using Co-Flow Jet (CFJ) Flow", doi: 10.13140/RG.2.1.1706.6007.

[16] G.-C. Zha, W. Gao, and C. D. Paxton, "Jet Effects on Coflow Jet Airfoil Performance," *AIAA Journal*, vol. 45, no. 6, pp. 1222–1231, 2007, doi: 10.2514/1.23995.

[17] J. Julian, W. Iskandar, F. Wahyuni, Ferdyanto, and N. T. Bunga, "Characterization of the Co-Flow Jet Effect as One of the Flow Control Devices," *Jurnal Asiimetrik: Jurnal Ilmiah Rekayasa & Inovasi*, vol. 4, no. 1, Jul. 2022, doi: 10.35814/asiimetrik.v4i1.3437.

[18] J. Zhang, K. Xu, Y. Yang, Y. Ren, P. Patel, and G. Zha, "Aircraft Control Surfaces Using Co-flow Jet Active Flow Control Airfoil," in *2018 Applied Aerodynamics Conference*, American Institute of Aeronautics and Astronautics, 2018. doi: doi:10.2514/6.2018-3067.

[19] C. Benoit, S. Péron, and S. Landier, "Cassiopee: A CFD pre- and post-processing tool," *Aerosp Sci Technol*, vol. 45, pp. 272–283, 2015, doi: https://doi.org/10.1016/j.ast.2015.05.023.

[20] A. Choudhry, M. Arjomandi, and R. Kelso, "A study of long separation bubble on thick airfoils and its consequent effects," *Int J Heat Fluid Flow*, vol. 52, pp. 84–96, Apr. 2015, doi: 10.1016/j.ijheatfluidflow.2014.12.001.

[21] S. M. A. Aftab, A. S. M. Rafie, N. A. Razak, and K. A. Ahmad, "Turbulence model selection for low reynolds number flows," *PLoS One*, vol. 11, no. 4, Apr. 2016, doi: 10.1371/journal.pone.0153755.

[22] M. Kandula and D. Wilcox, "An examination of k-omega turbulence model for boundary layers, free shear layers and separated flows," in *Fluid Dynamics Conference*, American Institute of Aeronautics and Astronautics, 1995. doi: doi:10.2514/6.1995-2317.

[23] A. Stagni, A. Cuoci, A. Frassoldati, T. Faravelli, and E. Ranzi, "A fully coupled, parallel approach for the post-processing of CFD data through reactor network analysis," *Comput Chem Eng*, vol. 60, pp. 197–212, 2014, doi: https://doi.org/10.1016/j.compchemeng.2013.09.002.

[24] H. Harinaldi, B. Budiarso, J. Julian, and A. WS, "Drag Reduction in Flow Separation Using Plasma Actuator in a Cylinder Model," 2015.

[25] Harinaldi, M. D. Kesuma, R. Irwansyah, J. Julian, and A. Satyadharma, "Flow control with multi-DBD plasma actuator on a delta wing," *Evergreen*, vol. 7, no. 4, pp. 602–608, 2020, doi: 10.5109/4150513.

[26] J. Julian, W. Iskandar, and F. Wahyuni, "Effect of Single Slat and Double Slat on Aerodynamic Performance of NACA 4415," 2022.

[27] J. Julian, W. Iskandar, F. Wahyuni, and F. Ferdyanto, "COMPUTATIONAL FLUID DYNAMICS ANALYSIS BASED ON THE FLUID FLOW SEPARATION POINT ON THE UPPER SIDE OF THE NACA 0015 AIRFOIL WITH THE COEFFICIENT OF FRICTION," *Media Mesin: Majalah Teknik Mesin*, vol. 23, no. 2, pp. 70–82, 2022.

[28] W. Iskandar, J. Julian, F. Wahyuni, F. Ferdyanto, H. K. Prabu, and F. Yulia, "Study of Airfoil Characteristics on NACA 4415 with Reynolds Number Variations," *International Review on Modelling and Simulations (IREMOS)*, vol. 15, no. 3, pp. 162–171, Jun. 2022.

[29] P. Kekina and C. Suvanjumrat, "A Comparative Study on Turbulence Models for Simulation of Flow Past NACA 0015 Airfoil Using OpenFOAM."